Journal of Materials Chemistry A

Accepted Manuscript

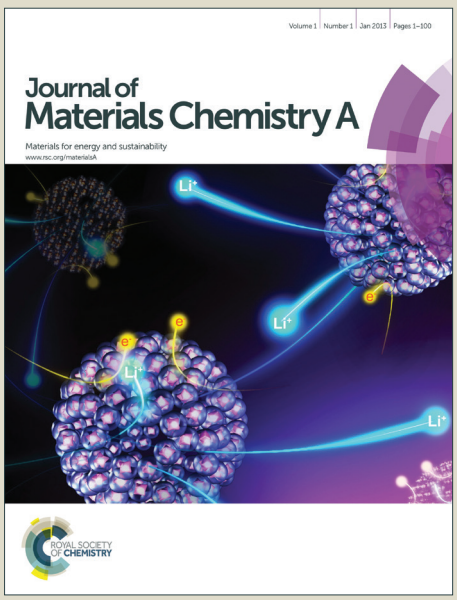

ROYAL SOCIETY OF CHEMISTRY

www.rsc.org/materialsA

Journal of Materials Chemistry A RSCPublishing

Paper

Sodium-Ion Battery Cathodes $Na_2FeP_2O_7$ and $Na_2MnP_2O_7$: Diffusion Behaviour for High Rate Performance

Cite this: DOI: 10.1039/x0xx00000x

Received 00th January 2012,
Accepted 00th January 2012

DOI: 10.1039/x0xx00000x

www.rsc.org/

John M. Clark,[a] Prabeer Barpanda,[b,c,d] Atsuo Yamada,[b,d] and M. Saiful Islam[a*]

The Na-ion battery is currently the focus of much research interest due to its cost advantages and the relative abundance of sodium compared to lithium. Recently, the pyrophosphate family of cathodes has attracted considerable attention, particularly $Li_2FeP_2O_7$ due to its high operating voltage and enhanced safety properties; in addition the sodium-based compounds $Na_2FeP_2O_7$ and $Na_2MnP_2O_7$ are also generating interest. Herein, we present defect chemistry and ion migration results, determined via atomistic simulation techniques, for $Na_2MP_2O_7$ (where M = Fe, Mn) as well as findings for $Li_2FeP_2O_7$ for direct comparison. Within the pyrophosphate framework the most favourable intrinsic defect type is found to be the cation anti-site defect, in which alkali-cations (Na/Li) and M ions exchange positions. Low activation energies are found for long-range diffusion in all crystallographic directions in $Na_2MP_2O_7$ suggesting three-dimensional (3D) Na-diffusion. In contrast $Li_2FeP_2O_7$ supports 2D Li-diffusion. The 2D or 3D nature of the alkali-ion migration pathways within these pyrophosphate materials means that antisite defects are much less likely to impede their transport properties, important for high rate performance.

1. Introduction

The portable energy storage market has been dominated by Li-ion batteries in the past two decades[1-7] due to their lightweight, high energy density and high power, which all depend critically on fast Li-ion mobility. Despite the wide-spread use of Li-ion cells, batteries based on alternative carrier ions such as sodium ions could be more suitable for large-scale energy storage systems. Whilst the higher gravimetric capacity afforded by Li-ion cells is critical for portable applications, the relative abundance and low cost associated with Na-ion batteries now make them an attractive alternative for grid storage.[8,9]

Substantial effort has been expended in previous decades to prepare electrode materials that can easily intercalate and transport Na-ions at suitable potentials. Among positive electrode materials, a variety of layered oxides (e.g. $NaxCO_2$, $NaCrO_2$, $NaVO_2$, $Nax[Fe_{0.5}Mn_{0.5}]O_2$) and polyanionic compounds (e.g. $NaFePO_4$, $Na_3V_2(PO_4)_3$, Na_2FePO_4F, $NaFeSO_4F$) have been reported[10-17].

Recently lithium pyrophosphate-based materials including $Li_2FeP_2O_7$ and $Li_2Fe_xMn_{1-x}P_2O_7$ ($0 \leq x \leq 1$) have been examined,[18-20] which show good electrochemical and thermal properties. It was found that $Li_2FeP_2O_7$ exhibited a redox-potential of 3.5 V vs Li/Li^+ while showing a reversible capacity of ~105 $mAhg^{-1}$,[18] whilst for the mixed-metal pyrophosphate it was found that the partial substitution with Mn was observed to increase the Fe^{3+}/Fe^{2+} redox potential.[19] This pyrophosphate structure can offer partial upshift of Fe^{3+}/Fe^{2+} redox potential approaching 4 V (vs Li/Li^+) independent of cationic size and redox activity of 3d metal substituants.[21] A universal Fe-redox upshifting near 4 V, the highest reported value matching the triplite $LiFeSO_4F$ cathode, can be registered in this $(PO_4)^{3-}$-oxyanionic system without using more electronegative and hygroscopic $(SO_4)^{2-}$ and/or F^- anions.[22] In addition to this high-voltage redox tunability, it is expected that the framework provided by the pyrophosphate anion will give rise to cathode materials with enhanced thermal stabilities.[23]

Motivated by the significance of Na-ion batteries for large-scale storage systems in addition to the promising properties of $Li_2FeP_2O_7$, attempts were made to synthesise a sodium version of the Fe-based pyrophosphate ($Na_2FeP_2O_7$),[24-26] as well as other Na-analogues with different transition-metal active redox species such as a new Mn-based polymorph, β-$Na_2MnP_2O_7$.[27,28] Yamada *et al.*[24] were able to prepare $Na_2FeP_2O_7$ via a conventional one-step solid-state synthesis, and found it to be electrochemically active, delivering a re-versible capacity of 82 $mAhg^{-1}$ with an operating voltage around 3 V (vs Na/Na^+). The combination of low cost materials, moderate theoretical capacity (~100 mAhg-1), high rate kinetics and good thermal stability makes $Na_2FeP_2O_7$ a highly promising Na-ion battery material. From a crystal structure view-point, the change of alkali ions from Li to Na results in different crystal

frameworks: while $Li_2FeP_2O_7$ adopts the monoclinic ($P2_1/c$) structure[18], $Na_2FeP_2O_7$ adopts the triclinic (P-1) structure[25].

Recently β-$Na_2MnP_2O_7$[27] has also been proposed as a new pyrophosphate cathode for sodium-ion batteries, and found to offer similar (if not slightly superior) electrochemical performance to $Na_2FeP_2O_7$. $Na_2MnP_2O_7$ displayed a discharge capacity close to 80 $mAhg^{-1}$ (at 25 ºC) with a voltage of 3.6 V, the highest Mn^{3+}/Mn^{2+} redox potential amongst all Mn-based cathodes. The electrochemical activity of the Mn-containing cathode material is noteworthy, when compared to the Li counterpart ($Li_2MnP_2O_7$), which is almost inactive at room temperature owing to its sluggish kinetics.[28] The β-$Na_2MnP_2O_7$ polymorph crystallise in the triclinic ($P1$) space group[27], isostructural to rose-polymorph of $Na_2CoP_2O_7$.[29]

The present study uses advanced simulation techniques to investigate important issues related to point defects and alkali (Na/Li) ion migration in $Na_2MP_2O_7$ (M = Fe, Mn, Co) and $Li_2FeP_2O_7$. The present work extends our previous simulation studies of lithium battery electrodes[30-39] such as $LiMPO_4$ (M = Mn, Fe, Co, Ni),[31-34] and our investigations of sodium-based cathodes such as $NaFeSO_4F$[36] and Na_2FePO_4F.[40] Herein, we present a systematic investigation of the defect chemistry, Na-ion migration paths and volume changes in $Na_2MP_2O_7$ (where M = Fe, Mn) with direct comparison with $Li_2FeP_2O_7$.

2. Simulation Methods

This investigation uses well established simulation techniques based on the Born model of solids. As these techniques are described in detail elsewhere[41,42], only a general outline will be given here. All systems were treated as crystalline solids, with interactions between ions consisting of a long-range coulombic component and a short-range component representing electron-electron repulsion and van der Waals interactions. The short-range interactions were modelled using the Buckingham potential,[41] and the well-known shell model[43] was employed to account for the polarizability effects. As argued previously, interatomic potential methods are assessed primarily by their ability to reproduce observed crystal properties. Indeed, they are found to work well, even for phosphate and silicate cathodes[31-36,39] where there is undoubtedly a degree of covalency. The Fe–O, Mn–O, P–O and O–O interatomic potentials were taken directly from the study of the related $Li_2FeP_2O_7$[39] (to which we compare our defect and migration results), whilst the Na–O potential was taken from the recent study of the Na_2FePO_4F[40] cathode material. The resulting potential parameters are listed in Table S1 (supporting information).

The lattice relaxation about defects (such as Na vacancies) and migrating ions was calculated by an implementation of the Mott-Littleton scheme incorporated in the GULP code[44], which partitions the crystal lattice into two separate regions, where ions in the inner region immediately surrounding the defect (~1000 ions) are relaxed explicitly. In contrast, the remainder of the crystal (~3000 ions), where the defect forces are relatively weak, is treated by more approximate quasi-continuum methods. It is worth noting that explicit relaxation of such a large number of lattice ions around defect species is not easily treated by electronic structure methods.

3. Results and Discussion

3.1 Structural Modelling

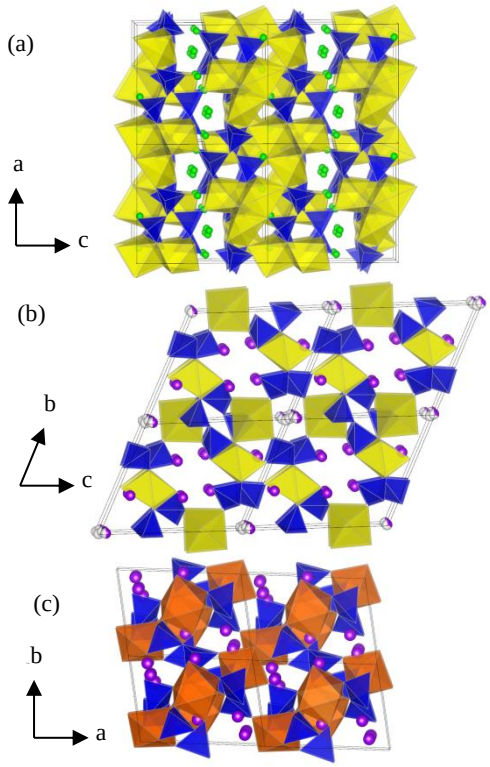

Fig. 1 Crystal structure of $Li_2FeP_2O_7$ and $Na_2MP_2O_7$ (M = Fe, Mn). a.) $Li_2FeP_2O_7$ ($P2_1/c$; c-axis view), b.) $Na_2FeP_2O_7$ (P-1; a-axis view), c.) $Na_2MnP_2O_7$ ($P1$; c-axis view); showing Li ions (green) Na ions (purple), FeO_6 octahedra (yellow), MnO_6 octahedra (orange) and P_2O_7 pyrophosphate (blue).

The starting point of the study was to reproduce the experimentally observed crystal structures (Figure 1). The structure exhibited by $Na_2FeP_2O_7$ is triclinic (P-1),[25] comprised of corner-sharing FeO_6 octahedra creating Fe_2O_{11} dimers, which are interconnected by both corner-sharing and edge-sharing with P_2O_7 pyrophosphate groups. The FeO_6 octahedra and PO_4 tetrahedra are connected in a staggered fashion thus creating large tunnels along the [011] direction within which the Na atoms are present. The Na ions occupy six distinct crystallographic sites; three of which are fully occupied (Na1, Na2, Na3), whilst the other three adopt sites that are partially occupied (Na4, Na5, Na6). Due to the partial occupancy it was necessary to use a 3×1×1 supercell approach considering different cation ordering schemes as used in previous simulations.[33,36,39] The energetics of the different cation configurations were investigated by performing a series of geometry optimizations in $P1$ symmetry. We note that the lattice energy differences were found to be very small (< 15 meV), sug-gesting that the ordering of the Na4, Na5 and Na6 sites may not be significant.

The structure exhibited by $Na_2MnP_2O_7$[27] consists of distorted MnO_6 octahedral and tetrahedral building blocks which are connected in a staggered manner thus creating tunnels along the [001] direction. The structures have corner-sharing isolated Mn_2O_{11} dimers, which are in turn connected by the P_2O_7 units by a mixed edge and corner-sharing fashion. The constituent Na atoms are located in eight inequivalent crystallographic sites. It has been postulated that the complex nature of this triclinic ($P1$) structure may allow for multidimensional Na^+ diffusion.[24] Comparisons between the

calculated and experimental crystal structures are given in Table 1.

Table 1 Calculated and Experimental Structural Parameters of $Na_2MP_2O_7$ (M = Fe, Mn) and $Li_2FeP_2O_7$.

Param	a (Å)	b (Å)	c (Å)	α (°)	β (°)	γ (°)
			$Na_2FeP_2O_7$			
calc.	6.449	9.483	10.993	64.85	86.24	73.13
expt.[25]	6.433	9.458	11.143	65.16	85.49	73.49
Δ (±)	0.016	0.025	0.150	0.31	0.75	0.36
			$Na_2MnP_2O_7$			
calc.	9.917	11.169	12.489	148.77	121.26	69.00
expt.[27]	9.922	11.084	12.473	148.39	121.95	68.42
Δ (±)	0.005	0.0854	0.0167	0.38	0.68	0.58
			$Li_2FeP_2O_7$[39]			
calc.	11.017	9.754	9.805	90.00	101.54	90.00
expt.	11.200	9.715	9.791	90.00	102.85	90.00
Δ (±)	0.183	0.039	0.014	0.00	1.31	0.00

For all pyrophosphate systems, the calculated unit cell parameters deviate from experiment by at most 0.18 Å, and in most cases much less; the same is found for the individual bond lengths. The excellent reproduction of the complex low symmetry monoclinic ($Li_2FeP_2O_7$) and triclinic ($Na_2MP_2O_7$) crystal structures gives us confidence that the interatomic potential models can be used reliably in subsequent defect and migration calculations.

3.2 Intrinsic Atomic Defects

Insights into the defect properties of cathode materials is crucial to the full understanding of their electrochemical behavior especially the possibility of "blocking" anti-site defects in structures showing 1D ion conduction. A series of isolated point defect (vacancy and interstitial) energies were calculated for both $Li_2FeP_2O_7$ and $Na_2MP_2O_7$ (M = Fe, Mn). By combining these energies, the relative energies of formation of Frenkel and Schottky-type defects were determined. These take the following general forms (using Kröger-Vink notation and where A = Li, Na):

A Frenkel: $$A_A^X \rightarrow V_A' + A_i^{\bullet} \quad (1)$$

M Frenkel $$M_M^X \rightarrow V_M'' + M_i^{\bullet\bullet} \quad (2)$$

O Frenkel $$O_O^X \rightarrow V_O^{\bullet\bullet} + O_i'' \quad (3)$$

Full Schottky $$2A_A^X + M_M^X + 2P_P^X + 7O_O^X \rightarrow 2V_A' + V_M'' + 2V_P''''' + 7V_O^{\bullet\bullet} + A_2MP_2O_7 \quad (4)$$

We also examined the A/M "anti-site" pair defect, which involves the exchange of an A^+ ion (Li^+ radius 0.76 Å, Na^+ radius 1.02 Å) with an M^{2+} ion (Fe^{2+} radius 0.78 Å and Mn^{2+} radius 0.83 Å)[45], according to:

M/A Antisite $$M_M^X + A_A^X \rightarrow A_M' + M_A^{\bullet} \quad (5)$$

This type of defect is worth investigating since anti-site or cation exchange effects have been observed in other examples of polyanionic systems including $LiMPO_4$ (M = Mn, Fe, Co, Ni)[31-33] and Li_2MnSiO_4[37].

Examination of the resulting defect energies listed in Table 2 reveals three main points. First, the magnitude of the energies suggests that formation of M Frenkel, O Frenkel and Schottky defects is unfavorable. In particular, O^{2-} vacancies and interstitials are highly unfavorable, and unlikely to occur in any significant concentration in the undoped materials, confirming the structural stability of the pyrophosphate framework in accord with thermal stability experiments[25].

Table 2 Energies of Intrinsic Atomic Defect Processes in $Na_2MP_2O_7$ (M = Fe, Mn) and $Li_2FeP_2O_7$.

		Energy (eV)		
Disorder Type	eq.	$Na_2FeP_2O_7$	$Na_2MnP_2O_7$	$Li_2FeP_2O_7$[39]
A Frenkel	(1)	1.14	1.34	1.21
M Frenkel	(2)	3.52	2.93	3.39
O Frenkel	(3)	3.53	3.92	3.99
Full Schottky	(4)	33.03	38.62	32.42
A/M anti-site	(5)	0.89	0.80	0.22

Second, the most favorable type of intrinsic defect for the $Na_2MP_2O_7$ material is found to be the Na/M anti-site pair as was predicted for the Li/Fe anti-site pair in the analogous study of the Li-analogue ($Li_2FeP_2O_7$)[39]. The formation energy for the Na/M antisite within the $Na_2MP_2O_7$ materials is of greater magnitude, suggesting lower but still significant concentrations of antisite defects within $Na_2MP_2O_7$. The concentration of anti-site disorder would be temperature dependent and hence sensitive to experimental synthesis conditions. Since Na^+ (radius 1.02 Å) is significantly larger than Li^+ (radius 0.76 Å), Fe^{2+} (radius 0.78 Å) and Mn^{2+} (radius 0.83 Å)[45], it is interesting to analyse the local structure of the anti-site defects revealed by the calculations.

Lastly, the second lowest energies for the $Na_2MP_2O_7$ cathode materials are found for the Na Frenkel defect (Table 2). This result is in accordance with the value calculated for the Li Frenkel defect within $Li_2FeP_2O_7$[39]. This suggests that a very minor population of such Li/Na vacancy and interstitial defects could be present at high temperatures. In the context of ion diffusion, the antisite defects bare more significance in the case of olivine materials as their presence blocks the only available 1D channel for alkali ion migration.[31,40]

3.3 Na Ion Migration

Examination of the Na^+ mobility and pathways in $Na_2MP_2O_7$ is of vital importance when considering their respective charge/discharge rates and any differences with Li^+ mobility. However, obtaining such insights for complex polyhedral structures is far from straightforward. Simulation methods can greatly enhance our understanding of the migration pathways and diffusion dimensionality at the atomic level.

Na-diffusion pathways were considered between all neighbouring Na positions within the $Na_2MP_2O_7$ (M = Fe, Mn) materials along each of the three principal axes via conventional vacancy hopping, as used in the study of Li-diffusion in $Li_2FeP_2O_7$[39]. Energy profiles for Na migration along each of the pathways considered can be mapped out, and the migration energies derived; such an approach has been used in numerous previous studies on oxide ion and cation migration in complex oxides.[31,32,46] The resulting lowest migration energies for Na diffusion along the three principal axes of the $Na_2MP_2O_7$ materials are reported in Table 3 with the corresponding lowest migration energies for Li diffusion within $Li_2FeP_2O_7$ reported for comparison[39].

Table 3 Calculated Migration Energies for Most Favourable Paths of Alkali-ion Diffusion: Na-ion Migration in $Na_2FeP_2O_7$ and $Na_2MnP_2O_7$ and Li-ion Migration in $Li_2FeP_2O_7$.

Net Diffusion Direction	Migration Energies (eV)		
	$Na_2FeP_2O_7$	$Na_2MnP_2O_7$	$Li_2FeP_2O_7$[39]
a-axis	0.33	0.58	0.73
b-axis	0.42	0.58	0.40
c-axis	0.49	0.58	0.40

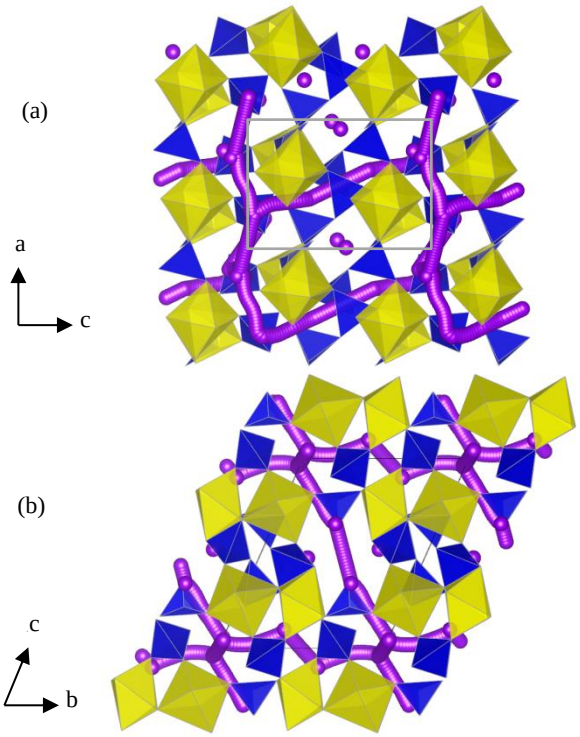

Fig. 2 Calculated paths for long-range Na^+ migration within $Na_2FeP_2O_7$ along the *a*-axis, *b*-axis and *c*-axis directions with activation energies ≤ 0.49 eV; a) view of the *ac*-plane; b) view of the *bc*-plane.

From the results presented in Table 3, it would appear that that both $Na_2MP_2O_7$ structures support quasi-three dimensional (3D) Na^+ diffusion with activation energies of 0.49 eV and 0.58 eV for $Na_2FeP_2O_7$, and $Na_2MnP_2O_7$ respectively. The final calculated paths for long-range Na^+ diffusion are shown in Figures 2 and 3. We note that in recent theoretical studies of a different $Na_2FeP_2O_7$ polymorph (triclinic, *P*1) Na^+ diffusion was found to be 2D with migration barriers of ~0.54 eV. The $Li_2FeP_2O_7$ compound shows 2D Li^+ diffusion in the *bc*-plane with activation energies of 0.40 eV.[39] Therefore in all cases the pyrophosphate framework appears to show high alkali-ion (Na^+/Li^+) mobility. Although there are no Li^+/Na^+ conductivity data for direct comparison, our calculated values for alkali-ion migration are consistent with experimental activation energies for Li/Na ion conductivity in other framework-structured phosphate materials.[47-49] The 2D and 3D transport behaviour in the pyrophosphates contrasts with that in olivine $LiFePO_4$ and $NaFePO_4$ which only allow Li^+/Na^+ migration along 1D channels parallel to the *b*-axis[31,40]. In addition, ion blocking by anti-site defects is much less likely to make a significant difference to the alkali (Na/Li) ion migration in these pyrophosphate materials. Electrochemical studies indicate that $Na_2FeP_2O_7$ has excellent rate kinetics, superior to that of $Li_2FeP_2O_7$[39]; this may be related to the high dimensionality (3D) and low migration energy for Na-ion diffusion in $Na_2FeP_2O_7$.

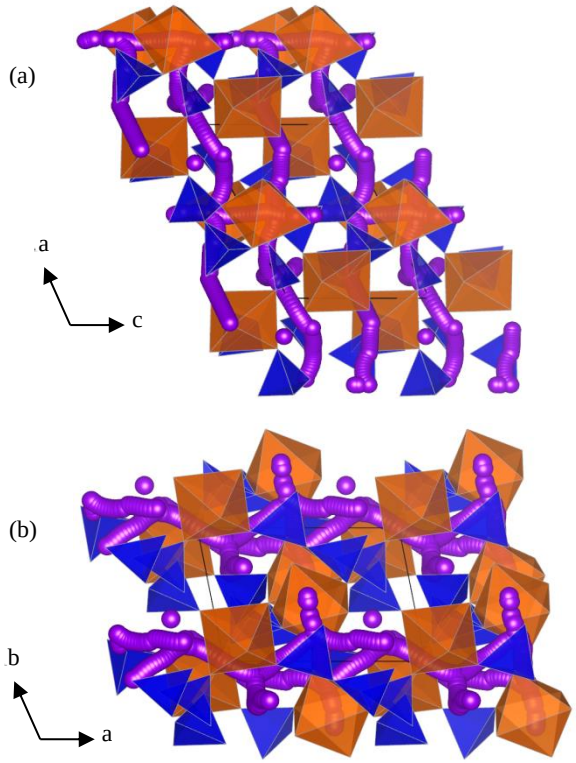

Fig. 3 Calculated paths for long-range Na^+ migration within $Na_2MnP_2O_7$ along the *a*-axis, *b*-axis and *c*-axis directions with activation energies ≤ 0.58 eV; a) view of the *ac*-plane; b) view of the *ab*-plane.

Our simulations also reveal curved paths between adjacent Na/Li sites within each of the pyrophosphate materials studied (Figures 2 and 3), which produces "wavelike" trajectories for long-range migration. It is worth noting that analogous, curved Li^+ migration paths were first predicted from atomistic simulation[31] of $LiFePO_4$, which were subsequently confirmed by neutron diffraction maximum entropy method (MEM) analysis.[50]

There has been recent debate about the volume difference between the reduced and oxidized phases as a significant factor in determining electrochemical performance of cathode materials.[40,51,52] For two-phase processes, a phase boundary between oxidized and reduced phases is formed during charge/discharge. Electrochemical performance could be affected by the amount of strain generated in this phase boundary, as well as by the activation energy barrier for Li-ion or Na-ion transport.

The difference in the unit cell volume (ΔV) of the oxidized and reduced phases is only ~3.26 % for $Na_2FeP_2O_7$, but > 15 % for $NaFePO_4$ and $NaFeSO_4F$. We note that while the majority of the compounds undergo volume contraction on Li/Na extraction, $Li_2FeP_2O_7$ shows a small volume expansion, although de(lithiation) has been found to be via a solid-solution mechanism in this pyrophosphate[52]. Although the interplay of all factors is still under investigation, materials with a large volume difference between the end member phases could lead to poor rate capability as discussed by Tripathi et al[40]. In contrast, promising electrochemical properties can be anticipated for Na-based cathode materials with low volume

change on cycling (e.g. < 7 %) and low ion migration activation barriers (e.g. < 0.5 eV) as in the case of $Na_2FeP_2O_7$ and Na_2FePO_4F.

4. Conclusions

We have investigated Fe- and Mn-based pyrophosphate materials which offer promising high rate cathodes that are potentially low cost and thermally stable for sodium-ion batteries. This systematic survey of $Na_2MP_2O_7$ (M = Fe, Mn) with comparison to $Li_2FeP_2O_7$ used atomistic simulation techniques to provide insights into their defect and ion migration properties. The main results can be summarized as follows:

(1) The atomistic simulations show good reproduction of the observed complex structures of $Na_2FeP_2O_7$ and $Na_2MnP_2O_7$. The defect calculations indicate the stability of the pyro-phosphate framework towards oxygen evolution, which is important for operational safety. The most favourable intrinsic defect type is the Na/M and Li/Fe antisite, with the relative energies suggesting greater Li/Fe disorder in the $Li_2FeP_2O_7$ material as observed.

(2) Both $Na_2FeP_2O_7$ and $Na_2MnP_2O_7$ are predicted to exhibit curved diffusion pathways parallel to the *a*-, *b*- and *c*-axes with low migration energies (~0.50 eV). Hence, the pyro-phosphate framework appears to support 3D Na^+ diffusion in $Na_2MP_2O_7$, (and 2D Li^+ diffusion in $Li_2FeP_2O_7$), which is consistent with the high rate kinetics observed for $Na_2FeP_2O_7$.

Acknowledgements

This work was funded by the EPSRC Supergen programme and made use of the high-performance computing service HECToR, via the HPC Materials Chemistry Consortium. PB thanks the Japan Society for the Promotion of Sciences for a JSPS Fellowship. VESTA[53] was used for analysis of results.

Notes and references

[a] Department of Chemistry, University of Bath, Bath, BA2 7AY, United Kingdom.

[b] Department of Chemical System Engineering, School of Engineering, The University of Tokyo, 7-3-1 Hongo, Bunkyo-Ku, Tokyo 113-8656, Japan.

[c] Materials Research Center, Indian Institute of Science, Bangalore 560012, India.

[d] Unit of Element Strategy Initiative for Catalysts & Batteries, ESICB, Kyoto University, Kyoto 615-8510, Japan.

† Electronic Supplementary Information (ESI) available: [details of any supplementary information available should be included here]. See DOI: 10.1039/b000000x/

1. M. Armand, J. M. Tarascon, *Nature* **2008**, 451, 652.
2. J. B. Goodenough, Y. Kim, *Chem. Mater.* **2010**, 22, 587.
3. B. L. Ellis, K. T. Lee, L. F. Nazar, *Chem. Mater.* **2010**, 22, 691.
4. M. R. Palacin, *Chem. Soc. Rev.* **2009**, 38, 2565.
5. C. Masquelier, L. Croguennec *Chem. Rev.* **2013**, 113, 6552.
6. V. Etacheri, R. Marom, R. Elazari, G. Salitra, D. Aurbach, *Energy Environ. Sci.* **2011,** 4, 3243.
7. Z. L. Gong, Y. Yang, *Energy Environ. Sci.* **2011,** 4, 3223.
8. B. L. Ellis, L. F. Nazar, *Curr. Opin. Solid State Mater. Sci.* **2012**, 16, 168.
9. V. Palomares, P. Serras, I. Villaluenga, K. B. Hueso, J. Carretero-Gonzalez, T. Rojo, *Energy Environ. Sci.* **2012**, *5*, 5884.
10. C. Delmas, J. J. Braconnier, C. Fouassier, P. Hagenmuller, *Solid State Ionics* **1981**, *4*, 165.
11. S. Komaba, C. Takei, T. Nakayama, A. Ogata, N. Yabuuchi, *Electrochem. Commun.* **2010**, *12*, 355.
12. N. Yabuuchi, M. Kajiyama, J. Iwatate, H. Nishikawa, S. Hitomi, R. Okuyama, R. Usui, Y. Yamada, S. Komaba, *Nat. Mater.* **2012**, *11*, 512.
13. P. Moreau, D. Guyomard, J. Gaubicher, F. Boucher, *Chem. Mater.* **2010**, *22*, 4126.
14. Z. L. Jian, L. Zhao, H. L. Pan, Y. S. Hu, H. Li, W. Chen, L. Q. Chen, *Electrochem. Commun.* **2012**, *14*, 86.
15. J. Barker, M. Y. Saidi, J. L. Swoyer, *Electrochem. Solid State Lett.* **2003**, *6*, A1.
16. B. L. Ellis, W. R. M. Makahnouk, Y. Makimura, K. Toghill, L. F. Nazar, *Nat. Mater.* **2007**, *6*, 749.
17. P. Barpanda, J. N. Chotard, N. Recham, C. Delacourt, M. Ati, L. Dupont, M. Armand, J. M. Tarascon, *Inorg. Chem.* **2010**, *49*, 7401.
18. S. Nishimura, M. Nakamura, R. Natsui, A. Yamada, *J. Am. Chem. Soc.* **2010**, *132*, 13596.
19. N. Furuta, S. Nishimura, P. Barpanda, A. Yamada, *Chem. Mater.* **2012**, *24*, 1055.
20. M. Tamaru, P. Barpanda, Y. Yamada, S. Nishimura, A. Yamada, *J. Mater. Chem.* **2012**, *22*, 24526.
21. T. Ye, P. Barpanda, S. Nishimura, N. Furuta, S. C. Chung, A. Yamada, *Chem. Mater.* **2013**, *25*, 3623.
22. P. Barpanda, M. Ati, B. C. Melot, G. Rousse, J. N. Chotard, M. L. Doublet, M. T. Sougrati, S. A. Corr, J. C. Jumas, J. M. Tarascon, *Nat. Mater.* **2011**, *10*, 772.
23. M. Tamaru, S. C. Chung, D. Shimizu, S. Nishimura, A. Yamada, *Chem. Mater.* **2013**, *25*, 2538.
24. P. Barpanda, T. Ye, S. Nishimura, S. C. Chung, Y. Yamada, M. Okubo, H. S. Zhou, A. Yamada, *Electrochem. Commun.* **2012**, *24*, 116.
25. P. Barpanda, G. Liu, C. D. Ling, M. Tamaru, M. Avdeev, S. C. Chung, Y. Yamada, A. Yamada, *Chem. Mater.* **2013**, *25*, 3480.
26. H. Kim, R. A. Shakoor, C. Park, S. Y. Lim, J. S. Kim, Y. N. Jo, W. Cho, K. Miyasaka, R. Kahraman, Y. Jung, W. J. Choi, *Adv. Funct. Mater.* **2013**, *23*, 1147.
27. P. Barpanda, T. Ye, M. Avdeev, S. C. Chung, A. Yamada, *J. Mater. Chem. A* **2013**, *1*, 4194.
28. C. S. Park, H. Kim, R. A. Shakoor, E. Yang, S. Y. Lim, R. Kahraman, Y. Jung, W. J. Choi, *J. Am. Chem. Soc.* **2013**, *135*, 2787.
29. F. Erragh, A. Boukhari, E. Elouadi, E. M. Holt, *J. Crystallogr. Spectrosc. Res.* **1991**, *21*, 321.
30. C. Eames, A. R. Armstrong, P. G. Bruce, M. S. Islam, *Chem. Mater.* **2012**, *24*, 2155.
31. M. S. Islam, D. J. Driscoll, C. A. J. Fisher, P. R. Slater, *Chem. Mater.* **2005**, *17*, 5085.
32. C. A. J. Fisher, V. M. H. Prieto, M. S. Islam, M. S. *Chem. Mater.* **2008**, *20*, 5907.
33. G. R. Gardiner, M. S. Islam, *Chem. Mater.* **2010**, *22*, 1242.
34. C. A. J. Fisher, M. S. Islam, *J. Mater. Chem.* **2008**, *18*, 1209.
35. A. R. Armstrong, N. Kuganathan, M. S. Islam, P. G. Bruce, *J. Am. Chem. Soc.* **2011**, *133*, 13031.
36. R. Tripathi, G. R. Gardiner, M. S. Islam, L. F. Nazar, *Chem. Mater.* **2011**, *23*, 2278.
37. N. Kuganathan, M. S. Islam, *Chem. Mater.* **2009**, *21*, 5196.
38. A. R. Armstrong, C. Lyness, P. M. Panchmatia, M. S. Islam, P. G. Bruce, *Nat. Mater.* **2011**, *10*, 223.
39. J. M. Clark, S. Nishimura, A. Yamada, M. S. Islam, *Angew. Chem. Int. Ed.* **2012**, *51*, 13149.
40. R. Tripathi, S. M. Wood, M. S. Islam, L. F. Nazar, *Energy Environ. Sci.* **2013**, *6*, 2257.
41. A. Walsh, A. A. Sokol, C. R. A. Catlow, *Computational Approaches to Energy Materials*. In Wiley-Blackwell, **2013**.
42. M. S. Islam, C. A. J. Fisher, *Chem. Soc. Rev.* **2014**, 43, 185.
43. B. G. Dick, A. W. Overhauser, *Phys. Rev.* **1958**, *112*, 90.
44. J. D. Gale, A. L. Rohl, *Mol. Simul.* **2003**, *29*, 291.
45. R. D. Shannon, *Acta Crystallogr.* **1976**, *A32*, 751.
46. M. S. Islam, P. R. Slater, *MRS Bull.* **2009**, *34*, 935.
47. C. Delacourt, L. Laffont, R. Bouchet, C. Wurm, J. B. Leriche, M. Morcrette, J. M. Tarascon, C. Masquelier, *J. Electrochem. Soc.* **2005**, *152*, A913.

48. J. Y. Li, W. L. Yao, S. Martin, D. Vaknin, *Solid State Ionics* **2008**, *179*, 2016.
49. L. Sebastian, J. Gopalakrishnan, *J. Mater. Chem.* **2003**, *13*, 433.
50. S. Nishimura, G. Kobayashi, K. Ohoyama, R. Kanno, M. Yashima, A. Yamada, *Nat. Mater.* **2008**, *7*, 707.
51. Y. Zhu, Y. Xu, Y. Liu, C. Luo, C. Wang, *Nanoscale* **2013**, 5, 780.
52. D. Shimizu, S. Nishimura, P. Barpanda, A. Yamada, *Chem. Mater.* **2012**, *24*, 2598.
53. K. Momma, F. Izumi, *J. Appl. Crystallogr.* **2008**, *41*, 653.